POLSKA AKADEMIA NAUK
INSTYTUT MASZYN PRZEPŁYWOWYCH

PRACE INSTYTUTU MASZYN PRZEPŁYWOWYCH

TRANSACTIONS
OF THE INSTITUTE OF FLUID-FLOW MACHINERY

70-72

WARSZAWA–POZNAŃ 1976
PAŃSTWOWE WYDAWNICTWO NAUKOWE

PRACE INSTYTUTU MASZYN PRZEPŁYWOWYCH

poświęcone są publikacjom naukowym z zakresu teorii i badań doświadczalnych w dziedzinie mechaniki i termodynamiki przepływów, ze szczególnym uwzględnieniem problematyki maszyn przepływowych

*

THE TRANSACTIONS OF THE INSTITUTE OF FLUID-FLOW MACHINERY

exist for the publication of theoretical and experimental investigations of all aspects of the mechanics and thermodynamics of fluid-flow with special reference to fluid-flow machinery

REDAKCJA – EDITORIAL OFFICE
Instytut Maszyn Przepływowych PAN
ul. Gen. Józefa Fiszera 14, 80-952 Gdańsk, skr. pocztowa 621, tel. 41-12-71

Printed in Poland

PAŃSTWOWE WYDAWNICTWO NAUKOWE – ODDZIAŁ W POZNANIU

Wydanie I. Nakład 630+90 egz. Ark. wyd. 63,25 Ark. druk. 49,25 Papier druk. sat. kl. V. 65 g., 70×100. Oddano do składania 4 VII 1975 r. Podpisano do druku w czerwcu 1976 r. Druk ukończono w czerwcu 1976 r. Zam. 528/118. H-16/245.
Cena zł 190,–

DRUKARNIA UNIWERSYTETU IM. ADAMA MICKIEWICZA W POZNANIU

III KONFERENCJA NAUKOWA

na temat

TURBINY PAROWE WIELKIEJ MOCY

Gdańsk, 24 - 27 września 1974 r.

*

IIIrd SCIENTIFIC CONFERENCE

on

STEAM TURBINES OF GREAT OUTPUT

Gdańsk, September 24 - 27, 1974

*

III НАУЧНАЯ КОНФЕРЕНЦИЯ

на тему

ПАРОВЫЕ ТУРБИНЫ БОЛЬШОЙ МОЩНОСТИ

Гданьск, 24 - 27 сентября 1974 г.

PRACE INSTYTUTU MASZYN PRZEPŁYWOWYCH
1976 Zeszyt 70 - 72

WIDEN TABAKOFF, AWATEF HAMED

USA*

Dynamics and Erosion Study of Solid Particles in a Cascade**

Nomenclature

$\bar{a}$ – particle acceleration,
$\bar{\alpha}$ – particle angular acceleration,
B – reference frame fixed in blades,
$\bar{b}$ – position vector of a particle in B,
β – angle between particle velocity and tangent to surface,
$\bar{c}$ – position vector of B_0 relative to E,
C_D – drag coefficient,
C_{D_0} – drag coefficient at Reynolds number less than 1.0,
C_p – specific heat of gas at constant pressure,
$\bar{D}$ – drag force on the particles,
d_p – particle mean diameter,
E – reference frame fixed in space,
E_0 – origin of the axes X, Y, and Z fixed in E,
$\bar{e}$ – position vector of p relative to axes fixed in E,
$g(Re)$ – correction function for the drag on sphere,
h – blade height,
m_p – mass of one particle,
μ_g – gas viscosity,
$\bar{n}_1, \bar{n}_2, \bar{n}_3$ – unit vectors in the direction of x, y, and z axes,
$\bar{N}_1, \bar{N}_2, \bar{N}_3$ – unit vectors in the direction of X, Y, and Z axes,
P – pressure force on spherical particles,
Re – Reynolds number,
t – time,
T_{g_0} – total gas temperature,
u, v, w – velocity in x, y and z directions,
V – velocity relative to blade,
x, y, z – axes fixed in B,
X, Y, Z – axes fixed in E,
ω – blade angular velocity,
ψ – a form of the stream function.

Subscripts

1 – before collision,
2 – after collision,
g – gas,
i – inlet to stator,
n – normal to surface,
p – particles,
t – tangent to surface.

Superscripts

B – relative to B,
B_0 – relative to the origin of the axes x, y, and z fixed in B,
E – relative to E,
p – particle position,
p^* – a point that coincides with p at a certain instance of time.

---

* Department of Aerospace Engineering, University of Cincinnati, Ohio.
** This work was sponsored under Grant Number DA-ARO-D-124-G-154, U. S. Army Research Office – Durham.

Introduction

This investigation was undertaken to determine a theoretical approach to calculate the dynamic behaviour of solid particles entrained by a gas flow in a two-dimensional stationary cascade of a turbine or a compressor blading. By dynamic behaviour, it is meant, the path the particles follow and their velocity histories through the passage taking into consideration both their collision with the blade surface and subsequent rebound from it.

The equations of motion of solid particles moving in a stream of gas were formulated assuming that the only force exerted on the particles is the drag force which causes the particles acceleration. In order to determine the solution of the equations of motion, information about the drag coefficient for spherical particles, the gas properties in the channel, the restitution ratio, and the rebound to incidence angle ratio were required.

Drag coefficient formulas for spherical particles were determined for different ranges of Reynolds number. The properties of the gas were calculated at all points of a square grid constructed in the cascade channel by solving numerically the equations of motion of gas flow in the cascade. The gas properties were assumed to be unchanged due to the presence of solid particles. Extensive experimental data was collected to study the collision and rebound phenomenon of the particles with the blade's wall. This data was used to determine formulas for the restitution and rebound to incidence angle ratios for the particles.

The effect of flow parameters such as particle mean diameter, particle material density, initial nondimensional particle velocity, and initial gas velocity on the particle trajectories and velocities are discussed.

From this research work one can calculate the energy lost due to impacts, the frequency of impacts at each location on the blade surface and create an erosion model of the blades. This will help to design turbomachine blades for optimum erosion as well as aerodynamic characteristics.

The study of particle trajectories in stationary flow fields in pipes and nozzles have been reported in many articles [1, 2, 3]. However, none of these investigations take into consideration the collision of particles with the wall or the cascade type flow. An experimental study [4] was made by the authors to determine the dynamic behaviour of solid particles in stationary cascades. The patterns of their trajectories and velocities were the same as predicted by the present study. The locations of the blade surface subjected to severe erosion as determined from this study, agrees with the physical observations of erosion tests made on cascades and real engine stators.

Drag force on a spherical particle moving in a stream of gas

Consider the motion of a spherical particle in a steady, very slowly moving incompressible gas flow. The inertia forces can be neglected compared to the viscous forces and, for no body forces, the Navier-Stokes equations become,

$$\operatorname{grad} P = \mu_g \nabla^2(\bar{V}_g). \tag{1}$$

The continuity equation of the gas may be written as

$$\operatorname{div}(\bar{V}_g)=0. \tag{2}$$

Taking the divergence of both sides of Equation (1) and using Equation (2) gives

$$\operatorname{div}\operatorname{grad} P=\nabla\cdot\nabla(P)=\nabla^2(P)=0. \tag{3}$$

Solving Equation (3) according to Durand [5], the pressure on the spherical particle surface is given by

$$P=-\frac{6\mu_g x|\bar{V}_{g\infty}|}{d_p^2}. \tag{4}$$

The velocity components of the gas u_g, v_g and w_g in the x, y and z directions can be determined from Equation (2) (Reference [5]). These velocity components are:

$$\begin{aligned} u_g&=|\bar{V}_{g\infty}|\left[\frac{3}{8}\frac{d_p x^2}{r^3}\left(\frac{d_p^2}{4r^2}-1\right)+1-\frac{1}{8}\frac{d_p}{r}\left(3+\frac{d_p^2}{4r^2}\right)\right],\\ v_g&=|\bar{V}_{g\infty}|\frac{3}{8}\frac{d_p xy}{r^3}\left(\frac{d_p^2}{4r^2}-1\right),\\ w_g&=|\bar{V}_{g\infty}|\frac{3}{8}\frac{d_p xz}{r^3}\left(\frac{d_p^2}{4r^2}-1\right), \end{aligned} \tag{5}$$

where

$$r=\sqrt{x^2+y^2+z^2}. \tag{6}$$

The shear force can be determined at every point on the surface of the sphere from the partial derivatives of Equations (5) at the wall. It may be shown that the resultant of the pressure differences relative to the undisturbed flow pressure and the friction forces has the same magnitude at all the points and equals

$$(3\mu_g|\bar{V}_{g\infty}|)/d_p.$$

Hence, the total drag force acting on the sphere can be determined by multiplying the given resultant force per unit area by the area of the surface of the sphere. This gives

$$\vec{D}=3\pi\mu_g d_p \bar{V}_{g\infty}. \tag{7}$$

If the particles are moving with a velocity $\bar{V}_p$ in a stream of gas moving with a velocity $\bar{V}_g$, the whole resistance force on the sphere may be written as,

$$\vec{D}=3\pi\mu_g d_p(\bar{V}_g-\bar{V}_p). \tag{8}$$

For higher Reynolds number, Equation (8) can not be considered valid, a correction for this equation which is a function of the Reynolds number was then required. The corrected Equation (8) has the form:

$$\vec{D}=3\pi\mu_g d_p(\bar{V}_g-\bar{V}_p)\,g(Re), \tag{9}$$

where

$$g(Re)=C_D\frac{Re}{24}=\frac{C_D}{C_{D_0}}. \tag{10}$$

In Equation (9) the Reynolds number dependent function $g(Re)$ has different forms depending on the range of the Reynolds number. It should have a value of one for Reynolds numbers less than 1.0. Its value can be determined theoretically from the solution of the Navier-Stokes equations for Reynolds numbers up to 4. The experimental data for drag coefficients on a sphere has to be used to determine $g(Re)$ for Reynolds numbers greater than 4 and within the practical limit of Reynolds number for particulate gas flow in turbomachines. Equation (10) shows that the function $g(Re)$ can be given as a ratio between the drag coefficient at any Reynolds number and the Stokes drag coefficient at small Reynolds number.

The formulas for the drag coefficient for spherical particles as defined in Equation (9) are given below for different ranges of the Reynolds number.

$$C_D=\frac{24}{Re}\qquad 0<Re\leqslant 1.0. \tag{11}$$

A solution of the Navier-Stokes equations of motion of a solid particle using a higher order term (Batchelor [6]) gives,

$$C_D=\frac{24}{Re}\left(1+\tfrac{3}{16}Re\right)\qquad 1.0<Re\leqslant 4{,}0. \tag{12}$$

The experimental data given by Schlichting [7] for the drag coefficient of spherical particles were fitted and the drag coefficient was given by

$$C_D=21.9416Re^{-0.718}+0.3240\qquad 4.0<Re\leqslant 2000. \tag{13}$$

For higher Reynolds number one may write,

$$C_D=0.4\qquad Re>2000. \tag{14}$$

The Reynolds number in Equations (11) through (14) is based on the particle mean diameter and the magnitude of the gas velocity relative to the particle or,

$$Re=\frac{d_p\,p_g}{\mu_g}\left|(\bar{V}_g-\bar{V}_p)\right|. \tag{15}$$

Detailed discussion of Equations (11) through (14) may be found in Reference [8].

Figure 1 gives the fitted drag curve as compared to the experimental results and it shows good agreement.

Equations of motion of solid particles entrained by the gas flow

In order to derive the equations of motion of solid particles entrained by gas flow in a cascade, it is convenient to define the axes systems as shown in Figure 1a.

The frame B is fixed in an arbitrary blade of the cascade with $\bar{n}_1$, $\bar{n}_2$ and $\bar{n}_3$ a set of non-parallel, noncoplanar, right handed unit vectors in the direction of the axes x, y and z, respectively. The point B_0, the origin of B, is taken to be the intersection of the plane tangent

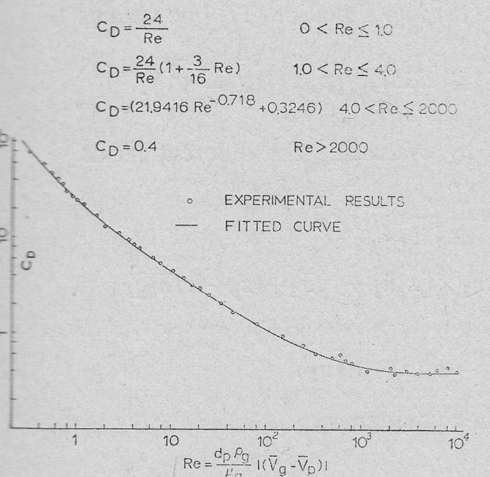

Fig. 1. Drag coefficient for spherical particle

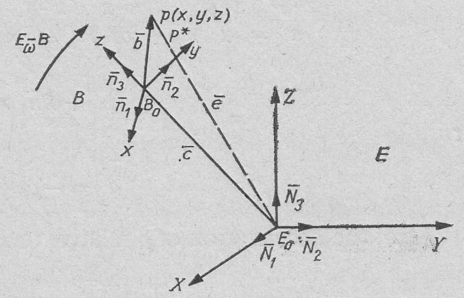

Fig. 1a

to the blade row at the entrance and the blade axial chord at the mid-plane that divides the blade height into two equal parts. Further, frame B moves with an angular velocity $\overset{E-B}{\omega}$ in a reference frame E fixed in space. In E, $\bar{N}_1$, $\bar{N}_2$ and $\bar{N}_3$ are unit vectors in the direction of the mutually perpendicular set of axes X, Y, and Z fixed at a point E_0, which is the intersection of the engine axis and a plane normal to it and tangent to the blade row at the entrance.

Consider the motion of a solid particle p in frame B. Let $\bar{b}$ be the position vector of p relative to B_0, $\bar{e}$ be the position vector of p relative to E_0, and $\bar{c}$ the position vector of B_0 relative to E_0 (see Fig. 1a).

From Fig. 1a, it can be shown [9, 10] that the acceleration of any particle p is given by

$$\overset{E-p}{a} = \overset{E-p^*}{a} + \overset{B-p}{a} + 2\,\overset{E-B}{\omega} \times \overset{B-p}{V}, \qquad (16)$$

where $\overset{E-p}{a}$ – the acceleration of p in E,

$\overset{E-p^*}{a}$ – the acceleration in E of a point p^* that coincides with p at the instant under consideration,

$\overset{B-p}{a}$ – the acceleration of p in the relative frame B,

$\overset{B-p}{V}$ – the relative particle velocity, and the last term in Equation (16) is the Coriolis acceleration of p.

According to Newton's second law of motion

$$m_p \overset{E-p}{a} = \bar{D}, \tag{17}$$

where m_p is the mass of one particle given by:

$$m_p = \frac{\pi d_p^3}{6} \bar{\rho}_p . \tag{18}$$

Now substituting Equations (9), (16) and (18) into Equation (17) one obtains

$$\overset{E-p}{a} = \overset{E-p*}{a} + \overset{B-p}{a} + 2(\overset{E-B}{\omega} \times \overset{B-p}{V}) = \left[\frac{18\mu_g}{\bar{\rho}_p d_p^2} g(Re)\right] (\overset{B-g}{V} - \overset{B-p}{V}). \tag{19}$$

Equation (19) can be further simplified by evaluating the different terms

$$\overset{E-p*}{a} = \overset{E-B}{\alpha} \times \bar{e} + \overset{E-B}{\omega} \times (\overset{E-B}{\omega} \times \bar{e}) = \frac{d}{dt}(-\omega \bar{n}_1) \times \bar{e}$$

$$+ \omega \bar{n}_1 \times \{\omega \bar{n}_1 \times [x_p \bar{n}_1 + y_p \bar{n}_2 + (z_p + R)\bar{n}_3]\}$$

or

$$\overset{E-p*}{a} = -\omega^2 y_p \bar{n}_2 - \omega^2 (z_p + R)\bar{n}_3 . \tag{20}$$

Also, the acceleration of p relative to B can be written as,

$$\overset{B-p}{a} = \ddot{x}_p \bar{n}_1 + \ddot{y}_p \bar{n}_2 + \ddot{z}_p \bar{n}_3 . \tag{21}$$

Furthermore, the Coriolis acceleration term can be reduced to

$$2(\overset{E-B}{\omega} \times \overset{B-p}{V}) = 2[(-\omega \bar{n}_1) \times (\dot{x}_p \bar{n}_1 + \dot{y}_p \bar{n}_2 + \dot{z}_p \bar{n}_3)]$$

or

$$2(\overset{E-B}{\omega} \times \overset{B-p}{V}) = 2\omega \dot{z}_p \bar{n}_2 - 2\omega \dot{y}_p \bar{n}_3 . \tag{22}$$

Substituting Equations (20), (21) and (22) into Equation (19), it reduces to,

$$\ddot{x}\bar{n}_1 + (\ddot{y}_p - \omega^2 y_p + 2\omega \dot{z}_p)\bar{n}_2 + [\ddot{z}_p - \omega^2(z_p + R) - 2\omega \dot{y}_p]\bar{n}_3$$

$$= \left[\frac{18\mu_g}{\bar{\rho}_p d_p^2} g(Re)\right] [(u_g - u_p)\bar{n}_1 + (v_g - v_p)\bar{n}_2 + (w_g - w_p)\bar{n}_3]. \tag{23}$$

Rearranging Equation (23) and defining the coefficient C which is a measure of the particles translational characteristic time as,

$$C = \frac{18\mu_g}{\bar{\rho}_p d_p^2} g(Re). \tag{24}$$

Equation (23) may take the expanded form,

$$\begin{aligned} \ddot{x}_p &= C(u_g - u_p), \\ \ddot{y}_p &= C(v_g - v_p) + \omega^2 y_p - 2\omega w_p, \\ \ddot{z}_p &= C(w_g - w_p) + \omega^2 (z_p + R) + 2\omega v_p . \end{aligned} \tag{25}$$

In Equations (25) the y distance is measured in a straight line and not a curve which limits the validity of the equations to the case where the radius R of the cascade row is relatively large. For the solution of the two-dimensional problem it is assumed that,

$$\omega=0, \quad w_p=w_g=0. \tag{26}$$

Substituting these assumptions into Equations (25), they reduce to

$$\ddot{x}_p=C(u_g-\dot{x}_p), \tag{27}$$

$$\ddot{y}_p=C(v_g-\dot{y}_p). \tag{28}$$

Equations (27) and (28) are the equations of motion of solid particles entrained by the gas flow in a two-dimensional stationary cascade. These equations are two ordinary non-linear differential equations that can be solved numerically for a given increment of time. The solution gives the x and y coordinates of the particle as well as its velocity components as it passes through the cascade channel.

Restitution ratio and rebound to incidence angle ratio for solid particles impinging the blade

In order to continue the solution of the equations of moiton of the particles after the point of collision with the blade, it was required to study the impact and rebound phenomenon of the particles and blade walls. The value of the particle velocity after rebound and the angle of rebound can be used as initial conditions in the equations of motion after impact. The loss in particle momentum due to collision can be found from the loss in its velocity which was termed "restitution ratio" and was defined as the ratio between the particle velocity after and before collision (V_{p2}/V_{p1}). The direction of the particle after it collides with the blade can be determined from the rebound to incidence angle ratio of the particle. This was defined as the ratio of the angle between the direction of the rebound particle velocity and the tangent to the blade surface at the point of impact and the angle between the direction of incoming particle velocity and the tangent to the blade surface at the point of impact (β_2/β_1). Since it was very difficult to predict theoretical formulas for these ratios, it was required to determine them empirically and examine their behaviours with the different flow parameters and particle and target materials.

Experiments were performed in which the gas particle flow tunnel [11] was used to inject particles of different sizes in the flow and photograph their impact with a set of blades fixed at the tunnel's test section. Particle diameters of 300, 1000 and 2000 microns were used. Particle material density $\bar{\rho}_p=68.7$ lb/ft^3 and the blades were made of stainless steel. The experiments showed primarily, that the restitution ratio and rebound to incidence angle ratio may be taken as a function of β_1 only. Other parameters seem to have little effect on these ratios. The results of these experiments are shown in Figs. 2 through 7. Figure 2 shows that the restitution ratio is independent of the velocity of the particle before impact, a decrease in restitution ratio is shown to be mainly due to an increase in β_1 as shown from the three curves in Fig. 2. Figure 3 shows that the restitution ratio is also independent of the place of collision; the distance x measured in the axial direction for which the gas velocity has different values at the suction as well as pressure sides of the blade. This means that the restitution ratio is not a function of the gas velocity at the point of collision. However, the higher the gas velocity, the higher will be V_{p_1} and hence V_{p_2} will have a higher value. Again β_1 has the more prominent effect. The data points in the plot of Figs. 2 and 3 are for particle diameters 300, 1000 and 2000 microns and they are uniformly distributed along the curves, which means that the restitution ratio is independent of the particle diameter. Similar results were reported [12] concerning the independence of V_{p_2}/V_{p_1} on d_p

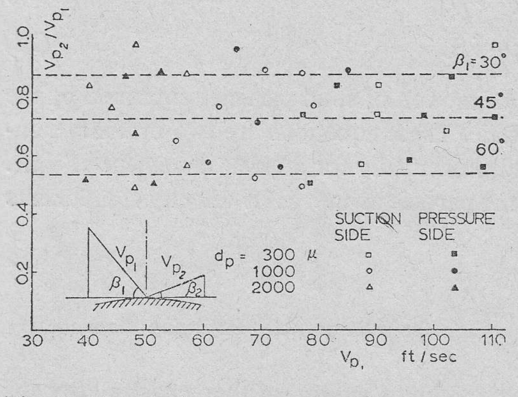

Fig. 2. Change in restitution ratio with V_{p_1}

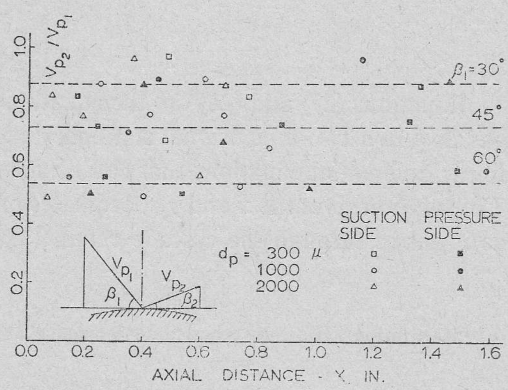

Fig. 3. Change in restitution ratio with x

for particle diameters from 15 to 300 microns. In Fig. 4 the ratio of the particle velocity tangent to the surface after and before collision were plotted versus β_1 and may be considered constant for all particle diameters. The dotted line was used to represent the data on Fig. 4 and may be expressed by the following equation

$$V_{pt2}/V_{pt1} = 0.95 + 0.00055\beta_1 . \tag{29}$$

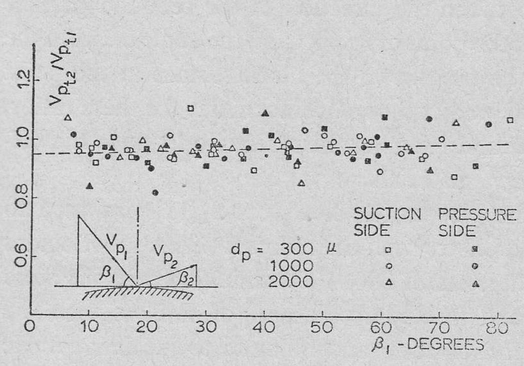

Fig. 4. Drop in particle relative tangential velocity due to collision

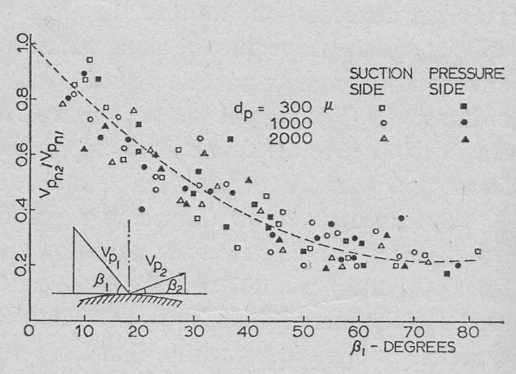

Fig. 5. Drop in particle relative normal velocity due to collision

The change in particle velocity due to impact is then mainly due to the contribution of the change in its normal velocity. The change in the ratio between particle velocity normal to the blade surface after and before collision as a function of β_1 is shown in Fig. 5 for different d_p. The dotted curve represents the data in the figure and may be written as follows:

$$\frac{V_{Pn2}}{V_{Pn1}} = 1.0 - 0.02108\beta_1 + 0.0001417\beta_1^2. \tag{30}$$

Equations (29) and (30) are sufficient to define the particle velocity and direction after collision. It may be convenient, hovewer, to determine directly curves that give the restitution ratio and the rebound to incidence angle ratio as a function of the incidence angle β_1.

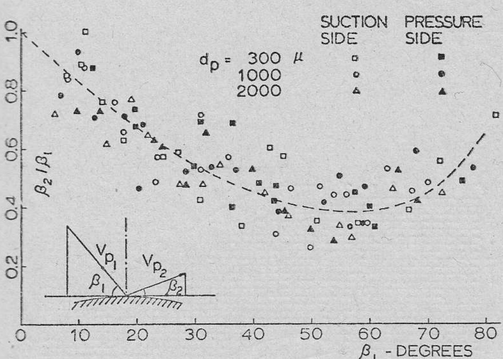

Fig. 6. Nondimensional angle of rebound

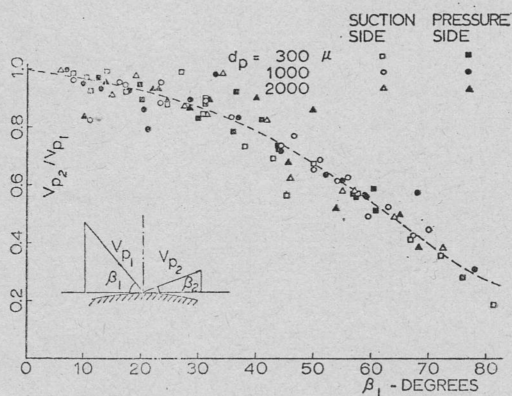

Fig. 7. Drop in particle relative velocity due to collision (restitution ratio)

Figure 6 gives β_2/β_1 as a function of β_1. The dotted curve is obtained by substituting Equations (29) and (30) into the following relation

$$\frac{\beta_2}{\beta_1} = \frac{1}{\beta_1}\cot^{-1}\left[\left(\frac{V_{Pt2}}{V_{Pt1}}\frac{V_{Pn1}}{V_{Pn2}}\right)\cot\beta_1\right]. \tag{31}$$

The restitution ratio versus β_1 is shown in Fig. 7. Equations (29) and (30) together with the following equation, were used to plot the dotted curve in Fig. 7

$$\frac{V_{p2}}{V_{p1}} = \frac{V_{Pn2}}{V_{Pn1}}\sqrt{\frac{1+\cot^2\beta_2}{1+\cot^2\beta_1}}. \tag{32}$$

Once the particles and blade materials are known, fundamental experiments can render the required information about the impact and rebound phenomenon. This information can then be used in the solution of the equations of motion of particles entrained by gas flow.

Gas flow properties in the cascade channel

Consider the nonviscous, irrotational, compressible steady gas flow moving in a stationary cascade of a turbomachine, the equations of motion [13] are:

1) Combined momentum and continuity equations.

$$\frac{\partial^2\psi}{\partial x^2} + \frac{\partial^2\psi}{\partial y^2} + \left[\frac{\partial(\ln R)}{\partial x} - \frac{\partial(\ln[h\rho_g])}{\partial x}\right]\frac{\partial\psi}{\partial x} - \frac{\partial(\ln[\rho_g])}{\partial y}\frac{\partial\psi}{\partial y} = 0. \tag{33}$$

where

$$u_g = -\frac{1}{h\rho_g}\frac{\partial\psi}{\partial y}, \tag{34}$$

$$v_g = \frac{1}{h\rho_g}\frac{\partial\psi}{\partial x}. \tag{35}$$

2) Combined state and energy equation

$$\frac{\rho_g}{\rho_{g_i}} = \left[1 - \frac{V_g^2}{2C_p T_i}\right]^{\frac{\gamma}{\gamma-1}}. \tag{36}$$

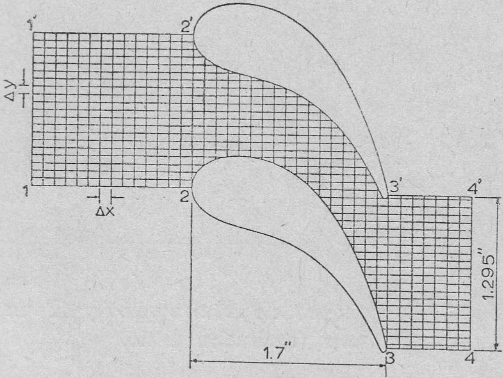

Fig. 8. Mesh points for turbine stator

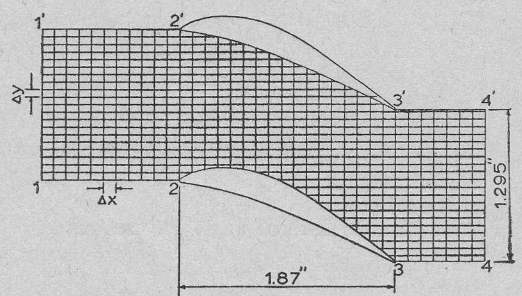

Fig. 9. Mesh points for compressor guide vane

Figures 8 and 9 show the mesh points in the cascade of a turbine and compressor blades respectively. The dimensions of the cascades are given on the respective figures. The computer program [14] was modified to give the solution of Equations (33) and (36), that is, the gas velocity in the x and y direction, u_g and v_g, as well as the gas density ρ_g at every mesh point and then store the data on magnetic tapes. These gas properties at the mesh points may be interpolated to give the gas condition at any point in the cascade channel. These values were needed to determine the step by step solution of Equations (27) and (28).

Numerical examples

The dynamic behaviour of solid particles suspended by gas flow in the turbine stator and the compressor guide vanes shown in Figs. 8 and 9, were calculated by solving the equations of motion of the particles, Equations (27) and (28). Cases where the particle mean diameter was given the values 1000, 200 and 40 microns, the particle material density was taken to be 34, 68.7 and 151 lb/ft^3 and the initial particle to gas velocity varied from 0.15 to 0.6 were considered. Calculation of these cases were used to study the effect of d_p, $\bar{\rho}_p$ and V_{p_i}/V_{g_i}, on the particle dynamic behavior. At a distance far upstream from the entrance to the turbine or compressor stators, the inlet gas flow conditions were: gas inlet velocity $V_{g_i} = 142.64$ ft/sec in the axial direction, the gas density $\rho_{g_i} = 0.076$ lb/ft^3 and the gas inlet total temperature $T_{g0}=60°F$. Gas flow properties, ρ_g, u_g and v_g at every mesh point were computed by solving Equations (33) and (36). The computer program given by the authors [15] may be used for the special case of two dimensional particle trajectories to determine the dynamic behaviours of the solid particle in the stators of the turbine and the compressor. The impact and rebound characteristics were described using Equations (31) and (32). The drag coefficient for spherical particles was represented by Equations (11) through (14), The results of this investigation are summarized in the next paragraph.

Turbine stator

The turbine blading of Fig. 8 was used in this study. Airfoil and cascade dimensions were given in References [16] and [8] respectively. The particles were assumed to enter the stator uniformly at a distance one inch upstream from the blade leading edge. Eleven particles were taken to enter the turbine stator at equal tangential distance apart. Figure 10 shows the trajectories of the eleven particles for $d_p=1000$ microns, while Fig. 11 shows the corresponding nondimensional velocity distribution of these particles. Similar curves for the trajectories and nondimensional velocities of eleven particles of mean diameters equal 40 microns are shown in Figs. 12 and 13, respectively. The first and the last particles were not taken exactly at the leading edge but slightly shifted in order to determine uniquely the direction of motion of the particle after collision. From Figs. 10 and 12, which show the particle trajectories for constant ρ_p and V_{p_i}/V_{g_i} it may be observed that, in general,

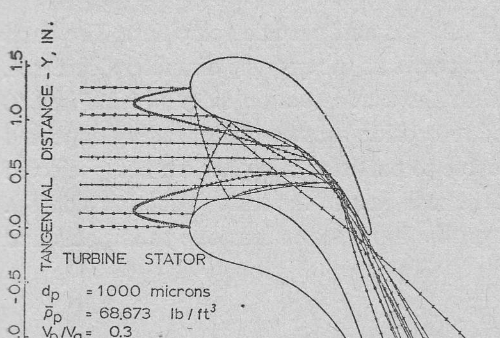

Fig. 10. Particle trajectories

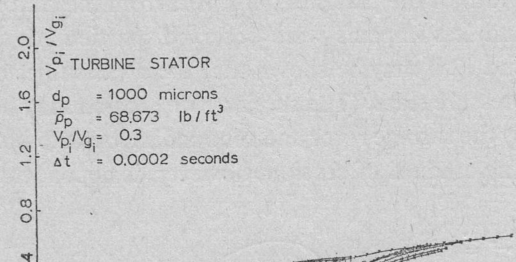

Fig. 11. Particle nondimensional absolute velocity

the particles can be divided into three main trajectory groups according to their initial place of impact[4]. The first group of particles are the ones that hit the upper part of the blade leading edge, travel laterally in the nozzle, may or may not hit the opposite blade pressure side, then move outside the nozzle. The second group consists of the particles that hit the pressure side of the blade then leave the nozzle. Finally, the last group of particles are the ones that hit the lower part of the leading edge, travel laterally and may or may not hit the opposite blade suction side or blade pressure side, then move away from the nozzle. It may be interesting to note that the fact a particle may or may not hit the opposite blade after hitting the blade leading edge and moving laterally, depends on the pitch, the blade camber and the solidity, which are geometrical considerations. Another factor is the mechanism of the impact and rebound phenomenon for a certain particle target material combination. Factors that measure the particles path deviation from the

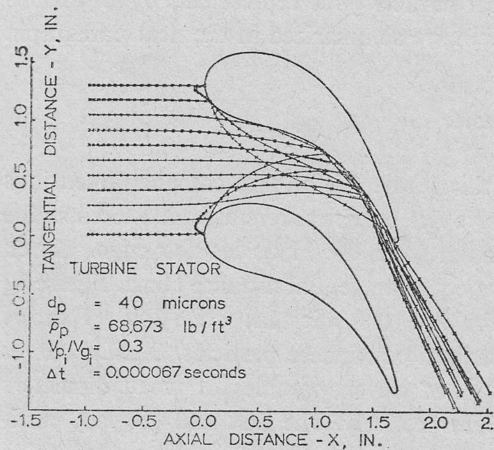

Fig. 12. Particle trajectories

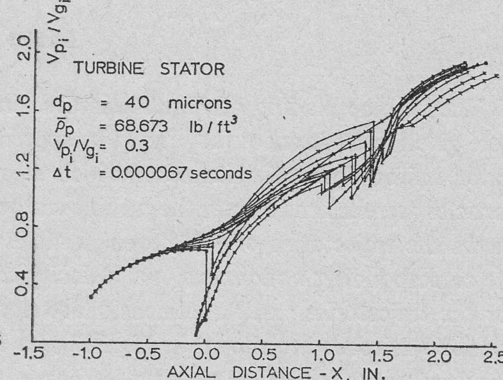

Fig. 13. Particle nondimensional absolute velocity

gas streamlines are the particle diameter, density and gas and particle velocities. The band width of the particles going out from the stator narrows as the particle diameter decreases, and less impacts were observed, particularly with the blade suction side. From Figs. 10 and 12 it may be shown that the areas subjected to erosion are the blade leading edge and pressure sides. (The suction side erosion may be due to particles of higher diameter rejected by the turbine rotor and rebounding back to hit the rear part of the stator's suction side[8]). The amount of erosion, however, is dependent on the momentum loss due to impacts and

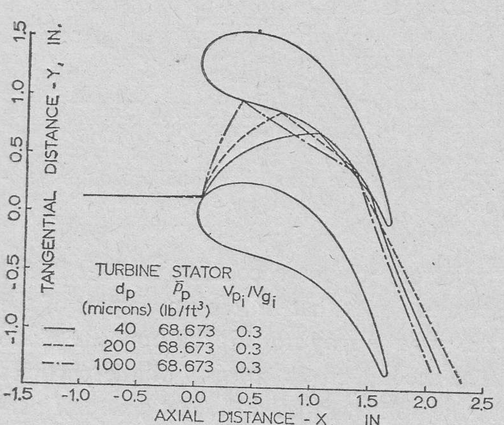

Fig. 14. Particle trajectories (effect of d_p)

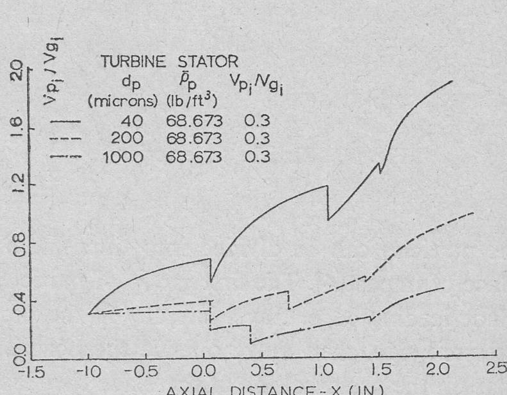

Fig. 15. Particle nondimensional absolute velocity (effect of d_p)

the frequency of impacts. Figures 11 and 13 show that the particles experience loss in momentum due to collision, the initial rate of increase of the particle velocity is higher for particles of smaller diameter and that the smaller diameter particles attain higher velocities. The particles tend to reach a corresponding constant velocity depending on their respective relaxation time.

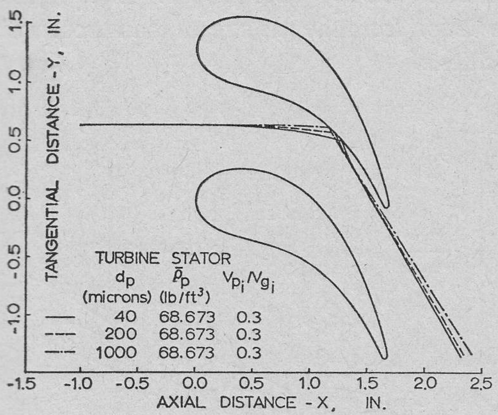

Fig. 16. Particle trajectories (effect of d_p)

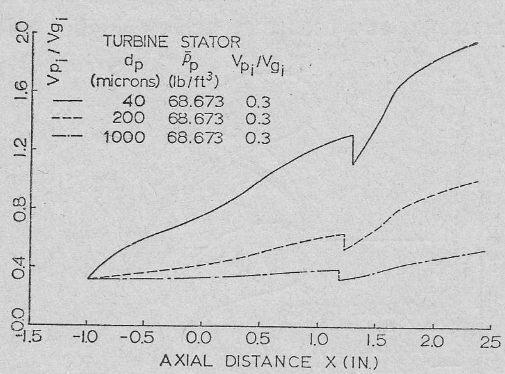

Fig. 17. Particle nondimensional absolute velocity (effect of d_p)

In order to show the effect of particle mean diameter, d_p, on the dynamic behavior, the three typical particle trajectory groups were considered. Figures 14, 16 and 18 show the trajectories of the three typical particles for d_p equals 1000, 200 and 40 microns while $\bar{\rho}_p$ and V_{pi}/V_{gi} remain constant, Figs. 15, 17 and 19 show the nondimensional velocity distributions of these particles. Figures 14, 16 and 18 show that particles of smaller diameters experience less lateral motion after colliding with the leading edge due to their smaller inertia, as the gas stream tends to force them to decrease their path deviation from gas streamlines. Figures 15, 17 and 19 indicate that particles with smaller diameters attain

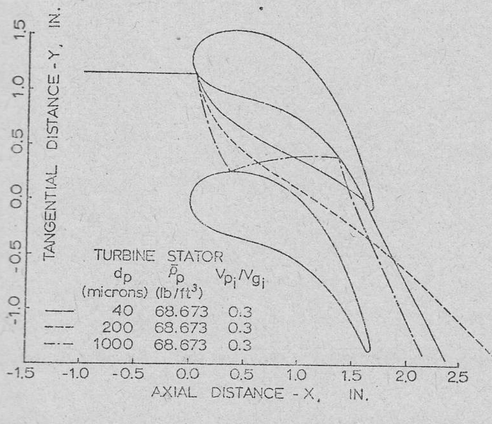

Fig. 18. Particle trajectories (effect of d_p)

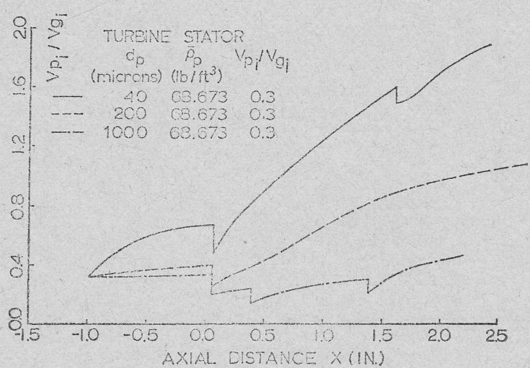

Fig. 19. Particle nondimensional absolute velocity (effect of d_p)

higher velocities in the same gas stream, while starting from the same initial velocity. Also, the velocity drop is a function of the respective angle of impact.

The effect of particle material density $\bar{\rho}_p$ on the dynamic behaviour of the solid particles for a typical trajectory type was illustrated by the trajectories of Fig. 20 for $\bar{\rho}_p=34$, 68.7 and 151 lb/ft^3, with a constant $d_p=200$ microns and a constant $V_{p_i}/V_{g_i}=0.3$. Figure 21 shows the corresponding particles nondimensional velocity distributions. These figures show the particles with smaller $\bar{\rho}_p$ have less deviation from the gas stream than those with higher $\bar{\rho}_p$ and that they achieve higher velocities.

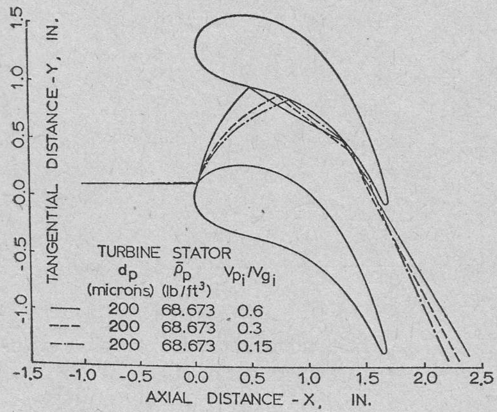

Fig. 20. Particle trajectories (effect of $\bar{\rho}_p$)

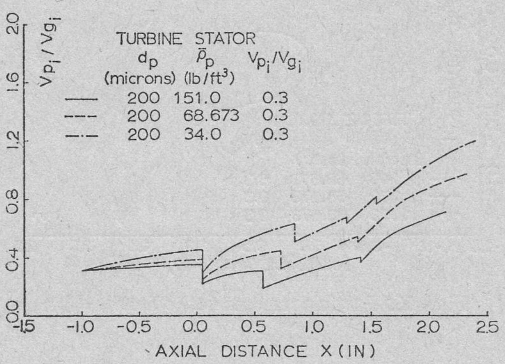

Fig. 21. Particle nondimensional absolute velocity (effect of $\bar{\rho}_p$)

The effect of the particle initial nondimensional velocity on the trajectories and velocities for one of the typical particle groups was shown in Figs. 22 and 23. Figure 22 shows the particle trajectories for $V_{p_i}/V_{g_i}=0.15$, 0.3 and 0.6, constant $d_p=200$ microns and constant $\bar{\rho}_p=68.7$ lb/ft^2. Figure 23 shows the velocities of these particles everywhere in the nozzle, nondimensionalized with respect to the initial gas velocity of the free undisturbed stream.

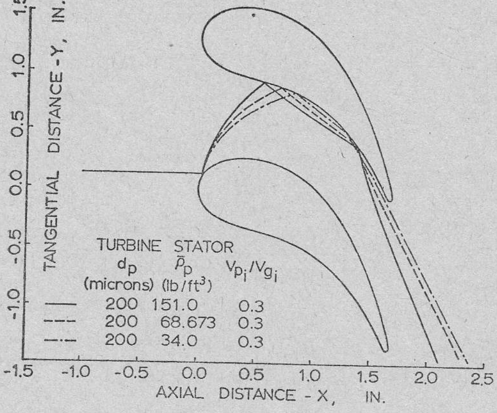

Fig. 22. Particle trajectories (effect of V_{p_i}/V_{g_i})

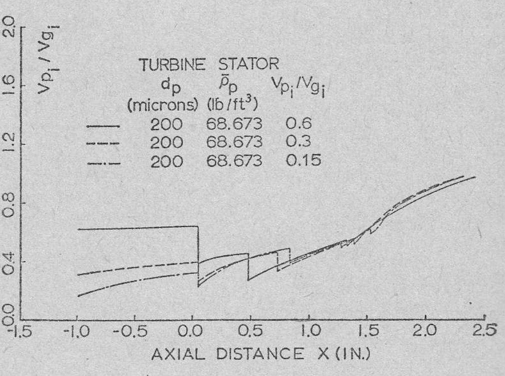

Fig. 23. Particle nondimensional absolute velocity (effect of V_{p_i}/V_{g_i})

The figures show that particles with smaller initial velocity experience less deviation from the gas streamlines due to their smaller inertia. The particles tend to reach the same respective velocity near the end of the nozzle irrespective of their velocity history. In the meantime, higher particle initial velocity relative to the gas corresponds to the case of smaller gas velocity relative to the particles. The effect of initial gas velocity would be that, higher gas initial velocity for particles entering the nozzle with the same, speed density and diameter, will cause the particles to follow more closely the gas streamlines and attain higher velocities. In general, it may be observed that particle mean diameter has more influence on the particle dynamic behavior than the particle material density. On the other hand, the initial particle velocity seems to have smaller effect on the particle behaviors since they tend to reach a constant velocity irrespective of the value of V_{p_i}/V_{g_i}.

Compressor guide vanes

The compressor blading of Fig. 9 was given in detail in Reference [8], while the airfoil dimensions were given in Reference [17]. This cascade was used in this investigation. Twelve particles were entered in the nozzle at a distance equal 0.88 inch upstream from the blade leading edge. The trajectories of these particles for $d_p = 1000$ microns, $\bar{\rho}_p = 68.7$ lb/ft^3 and $V_{p_i}/V_{g_i} = 0.3$ are shown in Fig. 24. Figure 26 shows the trajectories of similar groups of particles having the same $\bar{\rho}_p$ and V_{p_i}/V_{g_i} and for d_p of 40 microns. Figures 25 and 27 show the corresponding nondimensional velocity distribution. Due to the fact that compressor blades have smaller leading edges, the distance between the first two particles and the last two particles of Figs. 24 and 26 were taken smaller than the distances between other particles in order to show the groups of particles that hit the blade blunt leading edge. Particles are divided into four groups, the group that initially hit the upper part of the leading edge and move laterally, may or may not hit the opposite blade pressure

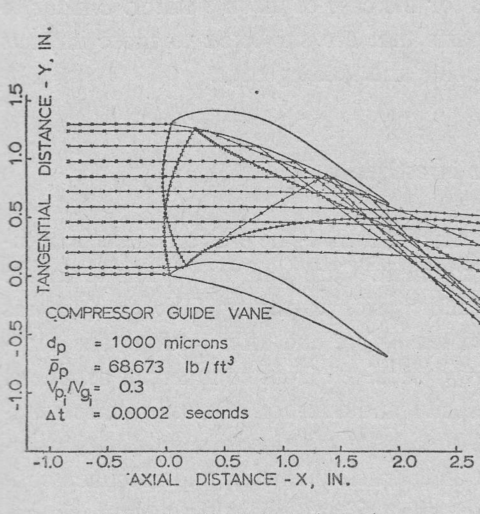

Fig. 24. Particle trajectories

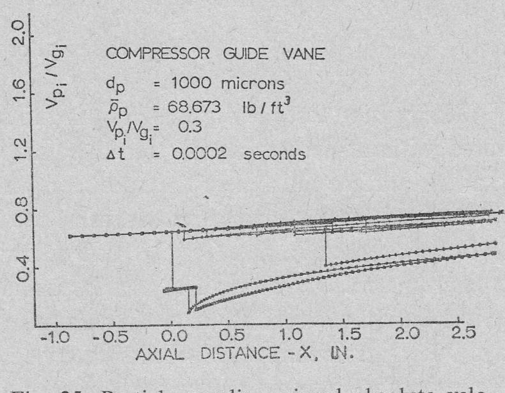

Fig. 25. Particle nondimensional absolute velocity

side then leave the nozzle. The second group are the particles that move without touching the blade surfaces. Because compressor quide vanes have smaller blade thickness and camber than a turbine stator, this group was not observed in the case of a turbine stator. The third group of particles hit the blade pressure side and then leave the nozzle. The final group hit the lower part of the leading edge and move laterally, may or may not hit the opposite blade suction side or blade pressure side, then leave the nozzle. It may be noticed that similar conclusions to that for the turbine stator case can be made for particles moving in compressor quide vanes with one additional observation, that the amount of impact is smaller for the case of compressor stator.

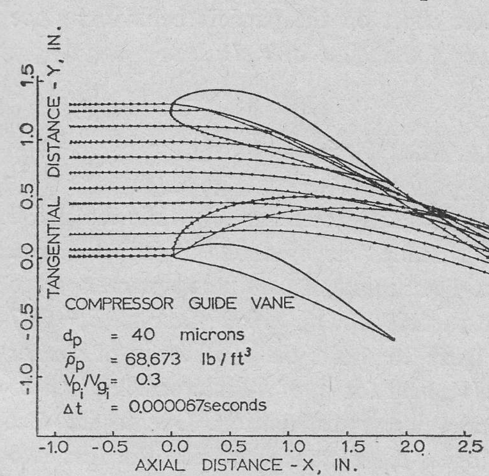

Fig. 26. Particle trajectories

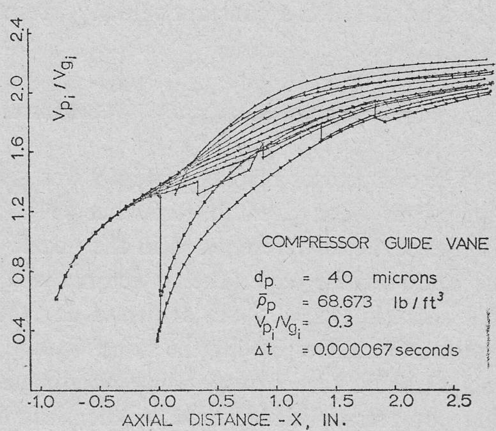

Fig. 27. Particle nondimensional absolute velocity

The effect of d_p, $\bar{\rho}_p$ and V_{p_i}/V_{g_i} on the dynamic behavior of the particles moving in a compressor quide vane are similar to the effects for the case of turbine stator. Similar to the case of turbine stator, compressor stator parts that are subjected to more impacts and hence more erosion, are the blade pressure side and leading edge.

Experimental erosion investigation

The erosion test facility was designed in such a manner that the erosion could be measured without destroying the aerodynamic environment. Care was also taken to insure that the surface finishes of the specimen were similar prior to testing. The erosion was determined by measuring the weight of the specimen before and after testing. The abrasives used were alumina (Al_2O_3) and quartz (SiO_2) obtained from commercial suppliers.

Parameters such as angle of attack, particle velocity, and duration of erosion can strongly influence the extent of the erosion damage and hence received close attention in this study. Other parameters such as particle concentration, particle diameter, and specimen configurations were tested sufficiently to determine the effect, if any, that they have on the results. For further information see Reference [18].

Effect of angle of attack

One of the more interesting features of erosion of ductile materials is the manner in which the angle at which particles strike the target surface influence the metal removal rate. Figure 28 illustrates these results for 2024 aluminum alloy at different particle velocities. For all of the velocities tested, the angle of maximum weight loss occurs at an angle of approximately 20 degrees. As the angle of attack increases from this value, the erosion reduces to a residual value at 90 degrees.

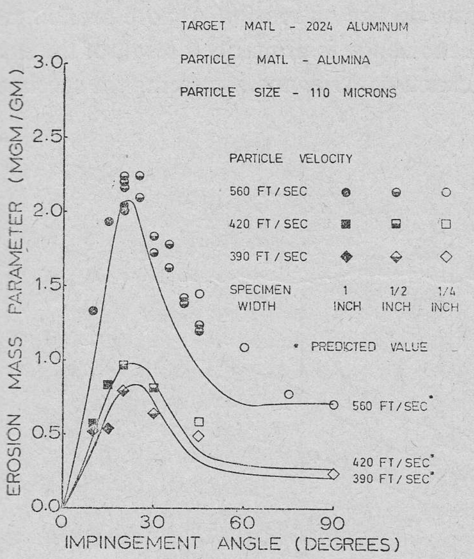

Fig. 28. Experimental and predicted erosion results

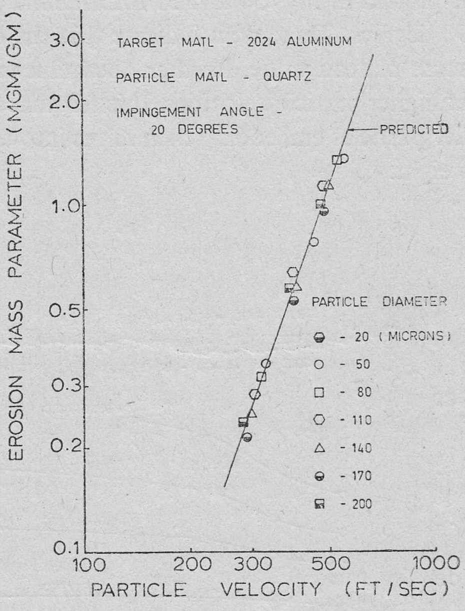

Fig. 29. Effect of velocity on erosion rate

Effect of particle velocity

The early investigators of erosion proposed that the process was proportional to the kinetic energy of the oncoming particle. This predicted relationship states that the erosion per unit mass of impacting particles is approximately proportional to the particle velocity on power two (i.e., $\varepsilon \sim V^2$). However, experimental observations have shown that the velocity exponent is normally greater than two. Some investigators found that a velocity exponent as high as three could be expected if the cutting depth of the particle is assumed as a function of the material strength. Finally, Sheldon and Kanhere [19] developed a particle penetration equation based on indentation hardness theory which predicts that the velocity exponent may be as high as three. Despite these analyses, the exact reason for the velocity exponent being greater than two is perhaps the single most controversial issue in the study of erosion.

The effect of velocity was investigated at angles of attack of 20 degrees and 90 degrees. These results are presented in Fig. 29. The influence at the other angles of attack was illustrated in Fig. 28. The data for 20 degrees impact indicate that the velocity exponent is approximately 2.8 (i.e., $\varepsilon \sim V^{2.8}$).

Effect of particle size

It has been found that the particle size can influence the rate of erosion. This parameter is plotted in Figs 30 and 31 for alumina particles at two different angles of attack; 20 and 90 degrees. These data indicate that the erosion damage increases with particle size up to some plateau value. Further, the influence of particle size on erosion is more pronounced at higher particle velocities. It is felt that this phenomenon is primarily a result of the smaller particles embedding themselves into the specimen material and increasing the specimen weight.

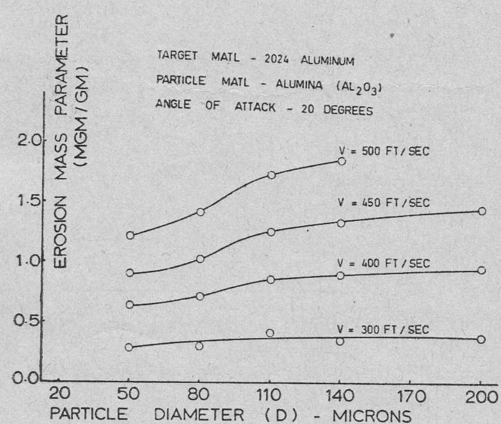

Fig. 30. Effect of particle diameter on erosion

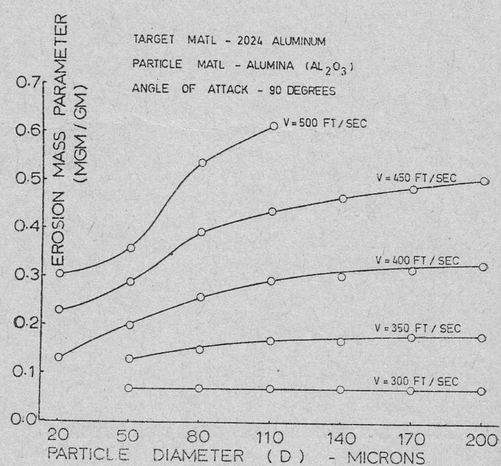

Fig. 31. Effect of particle diameter on erosion

Conclusion

For a given particle blade material combination, the restitution ratio and rebound to incidence angle ratio may be determined from fundamental test data. The equations of motion of particles entrained by gas flow in a turbine or a compressor stator were solved using the formulas describing the impact and rebound phenomenon, proper drag coefficient and gas conditions. The solution of the particle's equations of motion gives the particle trajectories and velocities in the cascade channel. The effect of particle mean diameter d_p, material density $\bar{\rho}_p$ and initial particle and gas velocities on particles dynamic behavior was discussed. A decrease in d_p, $\bar{\rho}_p$ or V_{pi}/V_{gi} or increase in initial gas velocity tends to stretch the trajectories in the axial direction. The particle mean diameter has more effect on the particles dynamic behavior than the particle material density. The initial gas and particle velocities have smaller influence. The parts of the blade subjected to the maximum amount of collisions, and hence, erosion damage are the blade leading edge and rear part of the pressure side. For a turbine stator three types of particle trajectories were observed while for compressor quide vanes the same three groups exist plus a group of particles that does not hit the blade at all. From the erosion experiments it was found that maximum erosion occurs at an angle of approximately 20 degrees. With the increase in the particle velocities and diameters the erosion increases. The results of this investigation, correlated with experimental erosion tests may be used to design turbomachinery stationary blades for optimum least erosion characteristics.

References

[1] C. E. Lapple and C. B. Shepherd, *Calculation of Particle Trajectories.* Industrial and Engineering Chemistry, Vol. 32, No. 5, May 1940, pp. 605 - 617.

[2] M. Gilbert, L. Davis and D. Altman, *Velocity Lag of Particles in Linearly Accelerated Combustion Gases.* Jet Propulsion, Vol. 25, January 1955, pp. 25 - 30.

[3] J. H. Neilson and A. Gilchrist, *An Analytical and Experimental Investigation of the Trajectories of Particles Entrained by the Gas Flow in Nozzles.* Journal of Fluid Mechanics, Vol. 35, Part 3, 1969, pp. 549 - 559.

[4] W. Tabakoff and M. F. Hussein, *Trajectories of Particles Suspended in Fluid Flow Through Cascades.* AIAA Journal of Aircraft, Vol. 8, No. 1, January 1971.

[5] W. F. Durand, *Aerodynamic Theory.* Vol. III, Berlin, Julius Springer 1935.

[6] G. K. Batchelor, *An Introduction to Fluid Mechanics.* Cambridge University Press, 1967.

[7] H. Schlichting, *Boundary Layer Theory.* McGraw-Hill, Inc., 1968.

[8] M. F. Hussein, *The Dynamic Characteristics of Solid Particles in Particulate Flow in Rotating Turbomachinery.* Ph. D. Dissertation, University of Cincinnati, Cincinnati, Ohio, 1972.

[9] A. W. Marris and G. E. Stoneking, *Advanced Dynamics.* McGraw-Hill, Inc., 1967.

[10] T. R. Kane, *Dynamics.* Hold, Rinhard and Winston, Inc., 1968.

[11] W. Tabakoff and M. F. Hussein, *Measurements of Particulated Gas Flow Pressure on Cascade Nozzles.* AIAA Journal of Aircraft, Vol. 8, No. 2, February 1971.

[12] W. J. Head and M. E. Harr, *The Development of a Model to Predict the Erosion of Material by Natural Contaminant.* Wear, An International Journal on the Science and Technology of Friction, Lubrication and Wear Vol. 15, No. 1, January 1970, pp. 1 - 40.

[13] M. H. Vavra, *Aero-Thermodynamics and Flow in Turbomachines.* John Wiley and Sons, Inc., 1960.

[14] T. Katsanis, *Computer Program for Calculating Velocities and Streamlines on a Blade to Blade Stream Surface of a Turbomachine.* NASA-TN D – 4525, April 1968.

[15] M. F. Hussein and W. Tabakoff, *Computer Program to Estimate the Dynamic Characteristics of Solid Particles Entrained by the Gas Flow in a Rotating Cascade of a Turbomachine.* Project Themis Report, University of Cincinnati, Cincinnati, Ohio, to be published.

[16] W. Tabakoff and M. F. Hussein, *An Experimental Study of the Effect of Solid Particles in the Pressure at the Blade Surface in Cascade.* United States Government Research and Development Report No. AD-703896.

[17] J. C. Emery, L. J. Heiring, J. R. Erwin and A. R. Felix, *Systematic Two Dimensional Cascade Tests of NACA 65 Series Compressor Blades at Low Speeds.* NACA Report No. 1368, 1958.

[18] W. Tabakoff and G. Grant, *Erosion Prediction in Turbomachinery Due to Environmental Solid Particles.* AIAA Paper No. 74 - 16, American Institute of Aeronautics and Astronautics 12th Aerospace Science Meeting, Washington, D. C., January 30-February 1, 1974.

[19] G. L. Sheldon and Kanhere, Ashok, *An Investigation of Impingement Erosion Using Single Particles.* Wear, 21 (1972) 195 - 209.

Badanie dynamiki cząstek stałych i ich erozyjne działanie w palisadzie

Streszczenie

Oblicza się trajektorie i prędkości cząstek stałych niesionych przez przepływ ściśliwy w palisadzie turbiny i sprężarki. Badano eksperymentalnie i uwzględniono przy rozwiązywaniu równań ruchu cząstek mechanizm zderzenia i odbicia cząstek stałych od ścianki łopatki. Badano wpływ średniej średnicy cząstek stałych, gęstości materiału, z którego są zbudowane oraz początkowych prędkości cząstek i gazu na ich charakterystyki dynamiczne w palisadzie. Ponadto przeprowadzono badania doświadczalne mające na celu znalezienie wpływu kąta padania, prędkości cząstek i ich rozmiarów na erozję łopatek. Przedyskutowano obserwacje dotyczące erozji łopatek.

Исследование динамики твердых частиц и эрозии в решетке

Резюме

Проводится расчет траекторий и скоростей твердых частиц в сжимаемом потоке, протекающем через турбинную или компрессорную решетку профилей. Экспериментально исследовался механизм ударов и отражений твердых частиц от стенки лопатки, который принимался во внимание при решениях уравнений движения частиц. Исследовалось влияние среднего диаметра твердых частиц, плотности материала, из которого они состоят, а также начальных значений скорости частиц и газа на их динамические характеристики в решетке. Кроме того, проводились экспериментальные исследования с целью определения влияния угла падения, скорости частиц и их размеров на эрозию лопаток. Обсуждаются результаты наблюдений эрозии лопаток.